Research in Astronomy and Astrophysics, 23:055015 (8pp), 2023 May https://doi.org/10.1088/1674-4527/acc91c

Nonlinearity Correction of Fourier Transform Spectrometer in Solar Observation Using Simulated Annealing

Ze-Yin Dong[1], Xian-Yong Bai[2,3], Song Feng[1], Yuan-Yong Deng[2,3], Zi-Hang Yu[1], Wen-Tong Ao[2,3], Xiao Yang[2,3], Zhi-Yong Zhang[2,3], and Zhi-Wei Feng[2,3]

[1] Faculty of Information Engineering and Automation, Kunming University of Science and Technology, Kunming 650500, China; feng.song@kust.edu.cn

[2] Key Laboratory of Solar Activity, National Astronomical Observatories, Chinese Academy of Sciences, Beijing 100101, China; xybai@bao.ac.cn

[3] School of Astronomy and Space Science, University of Chinese Academy of Sciences, Beijing 101408, China

Received 2022 October 12; revised 2022 December 24; accepted 2023 March 23; published 2023 April 26

Abstract

A Fourier transform spectrometer (FTS) has been used to observe solar activities due to its ultra-high spectral resolution. However, the FTS in-band spectra are usually distorted and some artifacts appear in out-of-band regions due to nonlinear effects. Therefore, the FTS nonlinear problem must be corrected. In this study, we proposed a novel method to correct the nonlinear effects using simulated annealing. We simulated several nonlinear spectra to evaluate the performance of our method. The calculated quadratic coefficients are extremely close to the given values, demonstrating that the method is effective and accurate. The proposed method is further used to correct the blackbody and solar spectra with nonlinearity obtained by Bruker IFS-125HR installed at the Huairou Solar Observing Station, which is a pathfinder for the accurate infrared magnetic field measurements of the Sun project. To the blackbody spectra, the nonlinearity in low- and high-frequency regions are corrected by 89.09% and 60.84%. The nonlinear correction of the solar spectra in the low- and high-frequency regions have reached 65.34% and 81.04%, respectively. These results prove that our method can correct the nonlinear problem to improve the data accuracy.

Key words: Sun: infrared – instrumentation: interferometers – techniques: interferometric

1. Introduction

Tens of physical parameters and their variations with the opacity are essential to reconstruct the dynamical three-dimensional solar atmosphere, which is a basis for analyzing a variety of quiet or active solar phenomena (Feng et al. 2020; Bai et al. 2021). Solar spectra obtained by a Fourier transform spectrometer (FTS) provide an effective way to quantitatively analyze the physical parameters because of the FTS ultra-high luminous flux, high spectral resolution, and wide bandpass (Griffiths 1983; Revercomb et al. 1988).

However, the time-based FTS has nonlinear effects due to moving mirror shaking, instrument operating temperature, too much photon flux on the radiation detector, or geometrical effects of the infrared beam (Griffiths 1983; Tobin et al. 2013). The nonlinearity not only causes the filtered wave band (called in-band spectra) of an observed spectra to be distorted but also decreases the spectral accuracy (Learner et al. 1996). Moreover, the artifacts appear in lower and higher wave band regions (called out-of-band spectra) because of the nonlinearity (Chase 1984). Therefore, the nonlinear correction must be made to obtain high-precise spectra.

The nonlinear correction methods include two types, electronic and algorithmic corrections. The electronic correction is to convert the FTS electronic-circuit structures (Bartoli et al. 1974; Schindler 1986; Carter et al. 1990). Whereas, the algorithmic correction minimizes the unexpected out-of-band radiations (Hoult & Ragusa 1987; Keens & Simon 1990; Carangelo et al. 1992; Curbelo 1993; Jeseck et al. 1998; Lachance 2000; Han et al. 2013; Minzhu et al. 2017).

A project called the accurate infrared magnetic field measurements of the Sun (AIMS) will be built in China. The FTS of AIMS will install a detector array of 64×2 to obtain the high-precise solar spectra in the mid-infrared wavelength. The FTS of AIMS spectral resolution reaches 0.6 Å, corresponding to $0.004\,\mathrm{cm}^{-1}$, in Mg I 12.32 μm that is the working spectral line (Bai et al. 2021). But now, we employed the Bruker IFS-125HR FTS with a point source detector as a temporary and simple experimental system at Huairou Solar Observing Station (HSOS), China. However, to the observed spectra from the FTS at HSOS, they usually exist the nonlinear effects. So we proposed a new method to correct the FTS nonlinear effects using the simulated annealing (SA) algorithm for high-accuracy.

This paper is structured as follows: Section 2 describes the nonlinear principles generated by the time-based FTS. Similarly, the SA algorithm is also described. In Section 3, several simulated spectra with nonlinearities are used to evaluate our method. The proposed method then corrects the blackbody and solar spectra obtained by the FTS at HSOS. Section 4 evaluates and discusses our method using quantitative comparison. Finally, our conclusion is given in Section 5.

2. Principle and Algorithm

2.1. Instrument Nonlinear Effect

The measured photon flux signal is called the interferogram in an FTS. Meanwhile, the relationship between the observed interferogram (I_m) and the ideal linear interferogram (I_i) is described by a Taylor series,

$$I_i = a_1 I_m + a_2 I_m^2 + a_3 I_m^3 + \cdots, \tag{1}$$

where a_1 is equal to unity and $a_i\,(i = 2,\ 3,...)$ denotes a polynomial coefficient. In case of an ideal linear system, $a_i (i > 1)$ are zero. Jeseck et al. (1998) concluded that interferograms usually have no significant cubic and higher order terms. Therefore, we only considered the quadratic term in our method.

An interferogram usually consists of a direct-current (DC) and an alternating-current (AC) component, i.e., $I_i = I_{i\_\mathrm{dc}} + I_{i\_\mathrm{ac}}$, $I_m = I_{m\_\mathrm{dc}} + I_{m\_\mathrm{ac}}$. Thus, Equation (1) is updated by:

$$I_{i\_\mathrm{dc}} + I_{i\_\mathrm{ac}} = (I_{m\_\mathrm{dc}} + I_{m\_\mathrm{ac}}) + a_2 (I_{m\_\mathrm{dc}} + I_{m\_\mathrm{ac}})^2. \tag{2}$$

The DC component is independent of the optical path difference (OPD) and its Fourier transform (FT) also has little effect on spectral analysis. Hence, I_{i_dc}, I_{m_dc} and $I_{m\_\mathrm{dc}}^2$ are removed and I_{m_ac} is merged, and Equation (2) is modified as,

$$I_{i\_\mathrm{ac}} = (1 + 2a_2 I_{m\_\mathrm{dc}}) I_{m\_\mathrm{ac}} + a_2 I_{m\_\mathrm{ac}}^2. \tag{3}$$

The FT of Equation (3) is defined as,

$$S_{i\_\mathrm{ac}} = (1 + 2a_2 I_{m\_\mathrm{dc}}) S_{m\_\mathrm{ac}} + a_2 S_{m\_\mathrm{ac}} \otimes S_{m\_\mathrm{ac}}, \tag{4}$$

where S_{i_ac} and S_{m_ac} are the FT components of I_{i_ac} and I_{m_ac}, respectively. The symbol $\otimes$ denotes a convolution operator. On the right of Equation (4), the first part is the distortion of the in-band spectra, and the second part is the out-of-band artifacts.

To an ideal spectrum without nonlinearity, its out-of-band regions are zero. Thus, the spectra of the out-of-band regions are defined as follows,

$$0 = (1 + 2a_2 I_{m\_\mathrm{dc}}) S_\mathrm{out} + a_2 S_\mathrm{out} \otimes S_\mathrm{out},\ S_\mathrm{out} \subseteq S_{m\_\mathrm{ac}}, \tag{5}$$

here S_out denotes the measured out-of-band spectra.

The nonlinearity is corrected by subtracting the quadratic component of an observed interferogram after obtaining the quadratic coefficient a_2. So an interval ($a_{2[vl,vh]}$) including the a_2 value is first obtained by using a small spectrum ($s_{[vl,vh]}$) in out-of-band regions, and the expression is as follows,

$$\begin{cases} a_\mathrm{temp} = -\dfrac{S_{[vl,vh]}}{S_{[vl,vh]} \otimes S_{[vl,vh]}}, & S_{[vl,vh]} \subseteq S_\mathrm{out}, \\ a_{2[vl,vh]} = -\dfrac{a_\mathrm{temp}}{1 - 2a_\mathrm{temp} I_{m\_\mathrm{dc}}}, & a_2 \in a_{2[vl,vh]}, \end{cases} \tag{6}$$

where I_{m_dc}, we considered the mean of the observed interferogram as the DC component.

Subsequently, we made the following objective function reach the minimum to obtain $\hat{a}_2$ which is a calculated quadratic coefficient. Meanwhile, the absolute value of $\hat{a}_2$ is highly close to a_2.

$$\hat{a}_2 = \arg\min_{a_2} \{(1 + 2a_2 I_{m\_\mathrm{dc}}) S_{[vl,vh]} + a_2 S_{[vl,vh]} \otimes S_{[vl,vh]}\},\ a_2 \in a_{2[vl,vh]}. \tag{7}$$

The SA algorithm (Kirkpatrick et al. 1983) retrieves $\hat{a}_2$ in $a_{2[vl,vh]}$ by making the right of Equation (7) reach the minimum.

2.2. Simulated Annealing

SA is an optimization process and retrieves the global optimal solution by making the objective function (f) convergent. It uses the Metropolis principle (Metropolis et al. 1953) process to determine the whole control parameters and the state transition of the optimal solution. The Metropolis principle avoids the algorithm falling into a local minimum,

$$\Delta f = f_i - f_j,\ P_{Tp}(\Delta f) = \begin{cases} 1, & \Delta f \leqslant 0 \\ \exp(-\dfrac{\Delta f}{KTp}), & \Delta f > 0 \end{cases}, \tag{8}$$

f_i and f_j represent an objective function f in state i and j, respectively. Δf denotes a reduction from f_i to f_j. K is a Boltzmann constant and Tp denotes the temperature parameter.

The SA parameters include initial temperature (Tp_0), Markov chain length (N), cool-down schedule (α), and stop criteria. Tp_0 is closely related to the final optimal solution and time-consuming of the entire algorithm. Therefore, it is set to 90 under considering the timeliness and the accuracy according to the Metropolis principle. N denotes the total iteration numbers at a temperature. The value is set to 1000 for precisely retrieving a_2. α is a temperature-drop parameter and affects the time-consuming of the entire algorithm. It is 0.98 in our method. The stop criterion is Tp_n close enough to zero, or the final optimal solution is found.

Our method executes N iterations at each temperature value. Each iteration process is as follows. First, select an initial value (x_0) randomly from $a_{2[vl,vh]}$ as an optimal solution ($\hat{x}$), and then use Equation (7) to calculate its objective function value. Second, select x_i randomly in x_0 neighborhood and calculate its objective function value. Subsequently, use the Metropolis principle to determine whether update $\hat{x}$. Stop if f

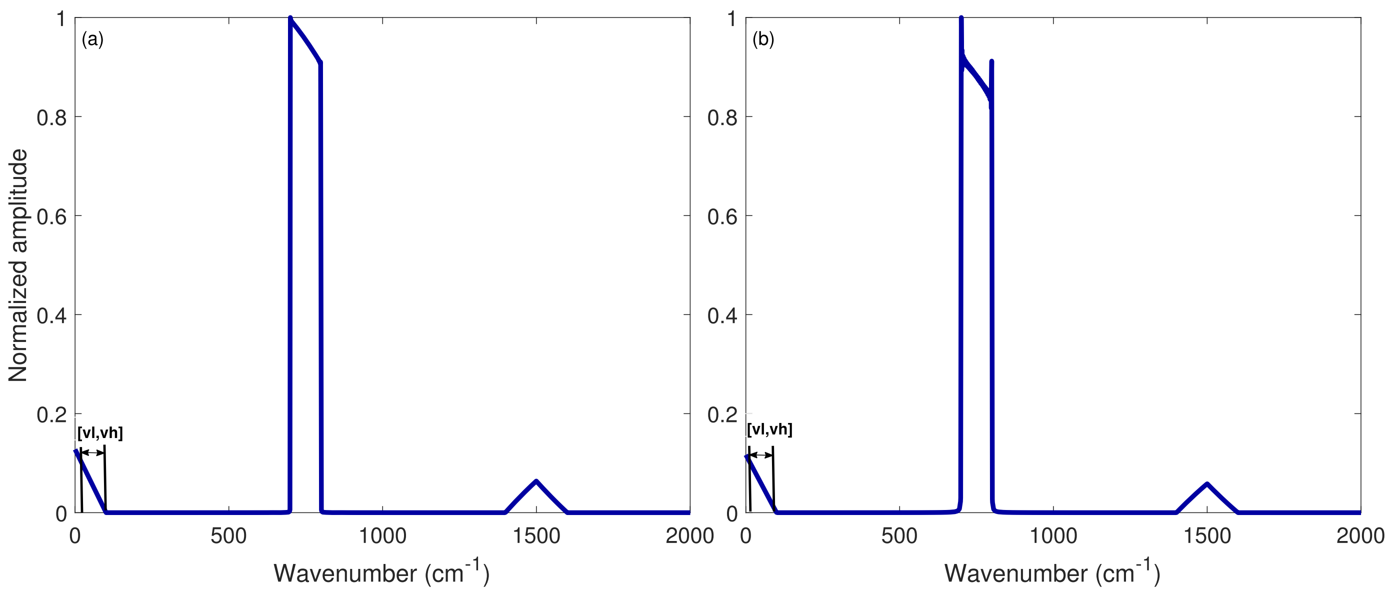

Figure 1. The nonlinear spectra with different spectral resolutions. (a) The nonlinear spectrum with the spectral resolution 1.3109 cm^{-1}. (b) The nonlinear spectrum with the spectral resolution 0.0041 cm^{-1}. Their filtered wave bands are 700–800 cm^{-1} and those artifacts are located in [0, 100] and [1400, 1600] cm^{-1}. The region from vl to vh cm^{-1} is used to retrieve $\hat{a}_2$.

has been converged, otherwise repeat this process for N times. Finally, update Tp_{n+1} according to αTp_n.

The entire method stops until Tp approaches zero, or f reaches convergence. The general description is listed as follows,

Method: The Nonlinear Correction Method using the SA Algorithm
Step 1 Get an interval $a_{2[vl,vh]}$ containing the "real" value of a_2;
Step 2 Give a random initial solution x_0 from $a_{2[vl,vh]}$ and set it as the initial optimal solution ($\hat{x}$);
Step 3 Repeat the following processes until $Tp \leqslant 0.1$.
Step 3.1 Execute the following process N (1000) times at each Tp until f is converged:
Step 3.1.1 Select a new solution (x_i) in the neighborhood of x_0;
Step 3.1.2 $\Delta f = f(x_i) - f(x_{i-1})$;
Step 3.1.3 If $\Delta f \leqslant 0$, thus $\hat{x} = x_i$. Otherwise $\hat{x} = x_i$ depends on $exp(-\frac{\Delta f}{Tp})$.
Step 3.2 Update T_p: $Tp_{n+1} = \alpha Tp_n$ ($\alpha = 0.98$), and reset N.
Step 4 Output $\hat{x}$.
Notation: x is the optimization variable, N the Markov chain length, n the nth iteration, Tp the temperature
parameter, and α the temperature-drop parameter.

3. Simulated Experiments and Applications

3.1. Simulated Experiments

We first simulated an ideal spectrum using the Planck formula of the blackbody radiation to evaluate our method,

$$B_v(T) = \frac{c_1 v^3}{\exp(\frac{c_2 v}{T}) - 1}, \tag{9}$$

where v denotes wavenumber and T is the blackbody temperature and set to 300 K. c_1 is $3.74 \times 10^{-8}\,\mathrm{W \cdot m^{-2} \cdot cm^4}$ and c_2 is $1.44\,\mathrm{cm \cdot K}$.

An ideal interferogram without DC is described by,

$$I(L) = \frac{1}{2}\sum_v B(v)\cos(2\pi v\delta)\Delta v, \tag{10}$$

where L and Δv denote the OPD and the spectral resolution, respectively.

The nonlinear interferogram with a quadratic component is defined as follows,

$$I_{\mathrm{nonlinear}} = I_{\mathrm{linear}} + a_2 I_{\mathrm{linear}}^2, \tag{11}$$

where I_{linear} and $I_{\mathrm{nonlinear}}$ denote the linear and nonlinear interferogram, respectively. a_2 is a given quadratic coefficient.

As mentioned above, we simulated a total of 24 data. The data have different quadratic coefficients and different wave bands in different resolutions. The coefficients are $6\times$, $7\times$, $8\times$, and 9×10^{-1} and the wave bands are located at [700, 800], [800, 900], and [900, 1000] cm^{-1}. Their spectral resolutions are 1.3109 and 0.0041 cm^{-1}. The data are generally classified into two different experiments, Simulated Experiment 1 and Simulated Experiment 2, according to the two spectral resolutions.

Figure 1 shows the spectra at 700–800 cm^{-1} with different spectral resolutions. The higher resolution, the more noticeable the spike at the step. Meanwhile, the nonlinear quadratic coefficients are both set to 6×10^{-1}. The spectra within ([0, 100] and [1400, 1600] cm^{-1}) are the quadratic artifacts.

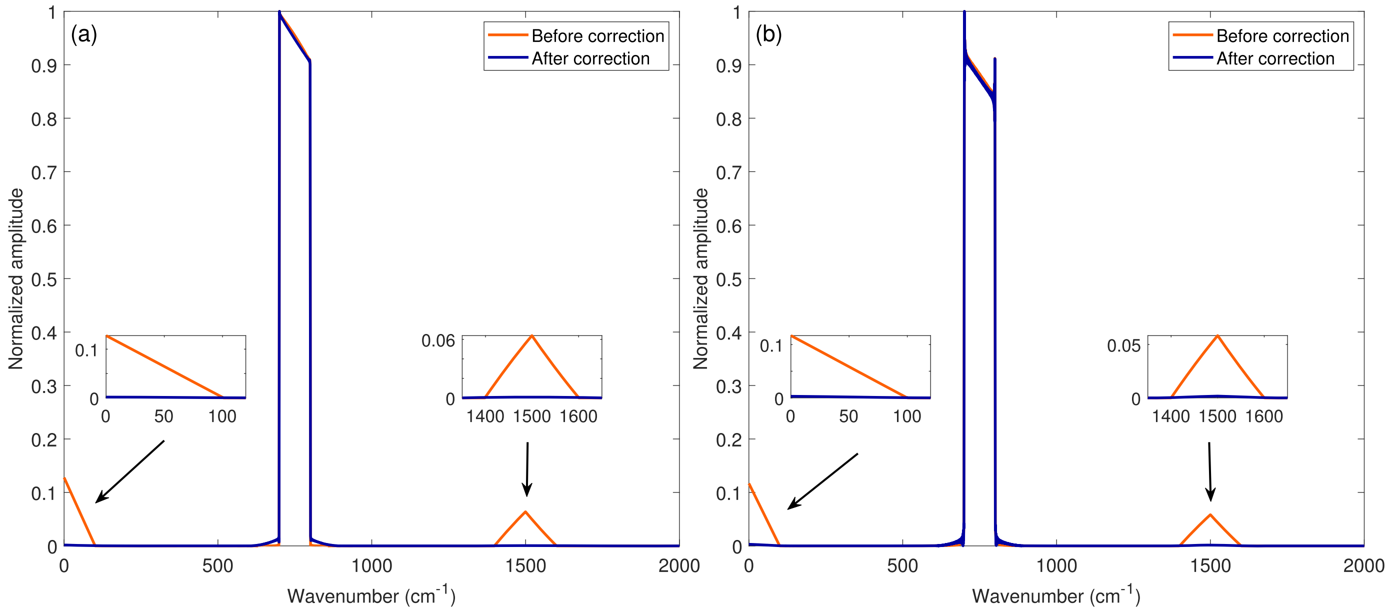

Figure 2. The spectra with resolution 1.3109 (a) and 0.0041 cm^{-1} (b). There, a_2 is 6×10^{-1}. The amplitudes of spectra after correction (blue) in [0, 100] and [1400, 1600] cm^{-1} are close to zero, meaning that the quadratic components have been eliminated fairly.

Table 1
The "Real" Values and the Quadratic Coefficient Calculated by SA

	Simulated Experiment 1				Simulated Experiment 2		
$\|a_2\| \times 10^{-1}$	[700, 800]	[800, 900]	[900, 1000]	$\|a_2\| \times 10^{-1}$	[700, 800]	[800, 900]	[900, 1000]
6.000	6.021	5.948	6.026	6.000	6.102	5.915	5.941
7.000	7.033	6.933	7.004	7.000	6.778	7.179	7.088
8.000	8.005	8.029	8.000	8.000	7.773	8.037	7.954
9.000	9.024	8.862	9.028	9.000	8.739	8.843	9.288

Whereas, the dual modulation phenomenon maybe affect the artifacts in the higher region (Chase 1984; Jeseck et al. 1998; Han et al. 2013). Therefore, we used the artifacts at *vl* and *vh* cm^{-1} in lower regions to retrieve the $\hat{a}_2$ value using our method.

After obtaining the $\hat{a}_2$ value, a nonlinear interferogram is corrected as follows,

$$I_{\rm corr} = I_{\rm nonlinear} + \hat{a}_2 I_{\rm nonlinear}^2. \tag{12}$$

In Figures 2 (a) and (b), compared with the spectra before correction (orange), the amplitudes of spectra after correction (blue) in [0, 100] and [1400, 1600] cm^{-1} are close to zero, meaning that the quadratic components have been corrected fairly. Table 1 lists all calculated quadratic coefficients of simulated data.

Meanwhile, as shown in Figure 3 (a), all optimization processes of different a_2 ($6\times$, $7\times$, and 8×10^{-1}) in same wave band ([700, 800] cm^{-1}) are converged quickly. Similar to Figure 3(a), all optimization processes shown in Figure 3(b) are converged after a total of 200 iterations. The same coefficient (9×10^{-1}) is in different wavebands. These results indicate that our method has good robustness.

Because the nonlinearity is corrected by subtracting the quadratic component from the nonlinear interferogram, which means the more accurate $\hat{a}_2$ the better the corrected result. In other words, the much smaller difference between the calculated $\hat{a}_2$ and the given value a_2, the better nonlinear corrected results.

For Simulated Experiment 1 of the same coefficient in different wave bands, e.g., 6.000×10^{-1}, $\hat{a}_2$ is very close to the given value a_2, where the mean difference is only 1.65%. Meanwhile, Simulated Experiment 1 of the same wave band of the different coefficients also achieve good performance, e.g., the mean difference of [700, 800] cm^{-1} is only 0.29%. In general, these results indicate that our method performs well on correcting the nonlinearity. The temperature factor also plays

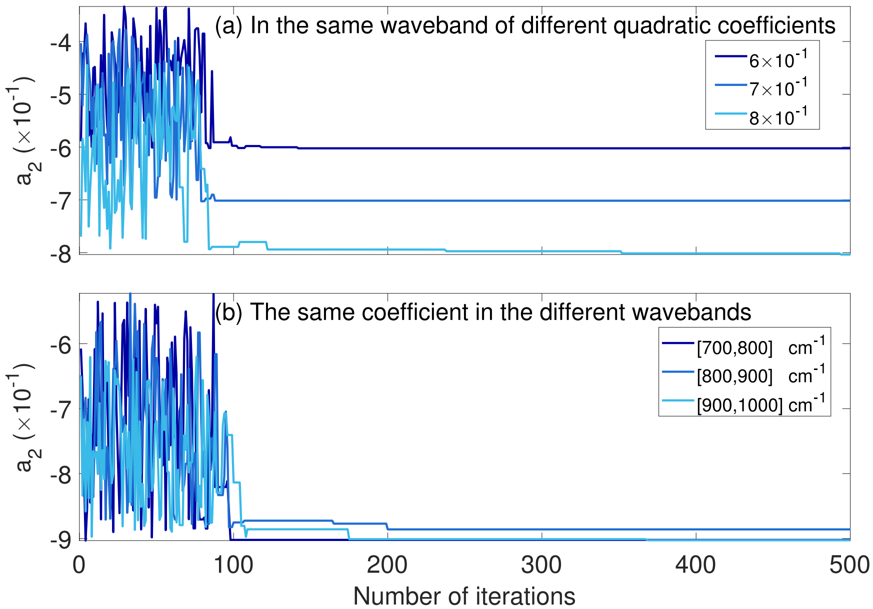

Figure 3. The convergences of our method. (a) The ([700, 800] cm^{-1}) wave band with different quadratic coefficients (6×10^{-1}, 7×10^{-1}, or 8×10^{-1}). (b) The same coefficient (9×10^{-1}) in different wave bands ([700, 800], [800, 900], or [900, 1000] cm^{-1}).

an important role in the FTS nonlinear effects. Therefore, we further evaluated the robustness of our method at different temperatures. All calculated coefficients listed in Table 2 are close enough to the given value, 6×10^{-1}. These results demonstrate that our method has good robustness in different temperature situations.

Table 2
The Same Coefficient (6×10^{-1}) at Different Temperatures

	Simulated Experiment 1	Simulated Experiment 2
300 K	6.002	6.102
310 K	5.937	6.041
320 K	6.070	6.108
330 K	6.114	6.071
340 K	6.007	5.977

3.2. Applications

To further evaluate the performance of our method, we corrected the blackbody spectra with nonlinearity obtained by the FTS at HSOS. Figure 4 shows the observed spectra at different temperatures.

The four out-of-band spectra within [0, 400], [1000, 1500], [2500, 3200], and [3800, 4600] cm^{-1} are also shown in Figure 4. The distributions in [0, 400] and [2500, 3200] cm^{-1} wave bands are generated by the two in-band spectra ([500, 900] and [1900, 2300] cm^{-1}). Similarly, the spectra within [1000, 1500] and [3800, 4600] cm^{-1} are also the quadratic artifacts. Different temperatures cause the different amplitudes of the quadratic artifacts. The lower the temperatures, the smaller the amplitudes.

Figure 5 shows the correction before (orange) and after (blue) at 750 and 800 °C, respectively. It is noted that both the amplitudes of the observed spectra and their corrected results have been normalized. In addition, all out-of-band spectra before and after correction are magnified.

In the terms of evaluation, we used the decrease of artifacts amplitudes before and after correction in out-of-band regions (P) to evaluate our method.

$$P = \left(1 - \frac{R_c}{R_m}\right) \times 100\%,\ P \in [0,\ 100\%], \tag{13}$$

where R_m and R_c denote the spectral amplitudes of before and after correction, respectively. The higher P, the better corrected result, and the nonlinearity is corrected completely when P equals 100%.

We used the mean of P in a small wave band ($\overline{P}$) to evaluate the correction effectiveness. $\overline{P}$ is defined as

$$\overline{P} = \frac{1}{M}\sum_{i=1}^{M} P_i,\ i = 1,\ 2, \cdots,\ M. \tag{14}$$

The nonlinearity in [0, 400] cm^{-1} is corrected by 89.09%, those in [1000, 1500] cm^{-1} corrected by 72.22%, in [2500, 3200] cm^{-1} by 83.11%, and by 60.84% in [3800, 4600] cm^{-1} of Figure 5 (a). Similar to Figure 5 (a), the nonlinear effects in those wave bands are corrected by 87.80%, 72.50%, 80.44%,

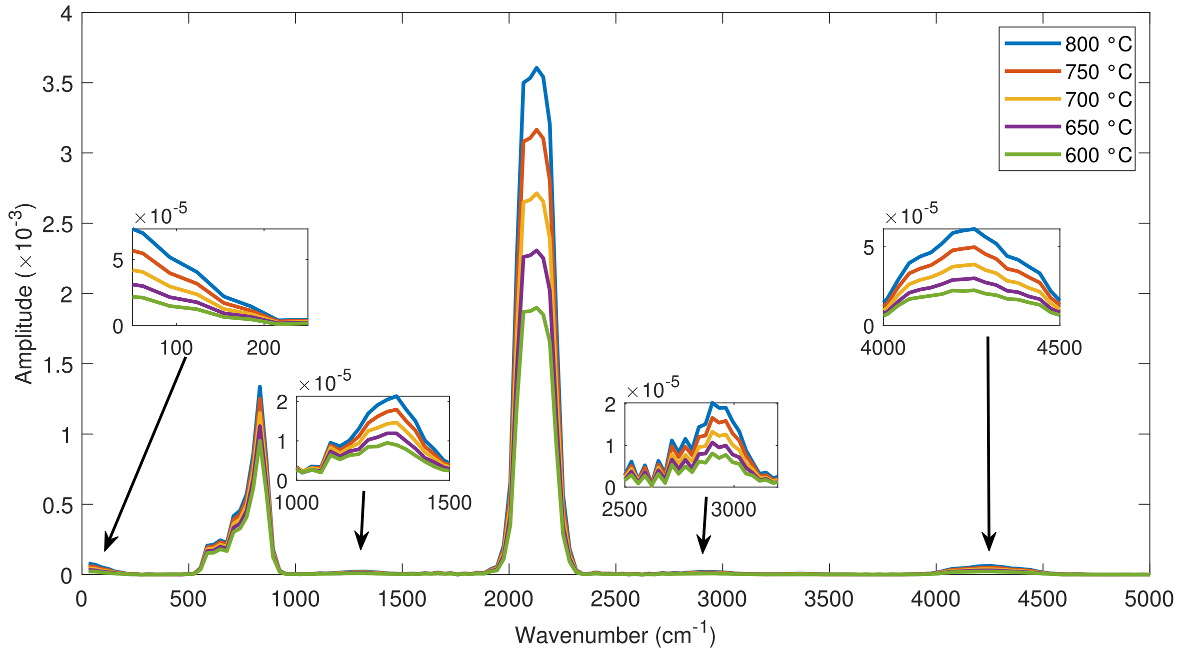

Figure 4. The observed spectra with nonlinearity at different temperatures obtained by the FTS at HSOS, and the corresponding filtered wave bands are [500, 900] and [1900, 2300] cm^{-1}. The four artifacts within [0, 400], [1000, 1500], [2500, 3200], and [3800, 4600] cm^{-1} in out-of-band regions.

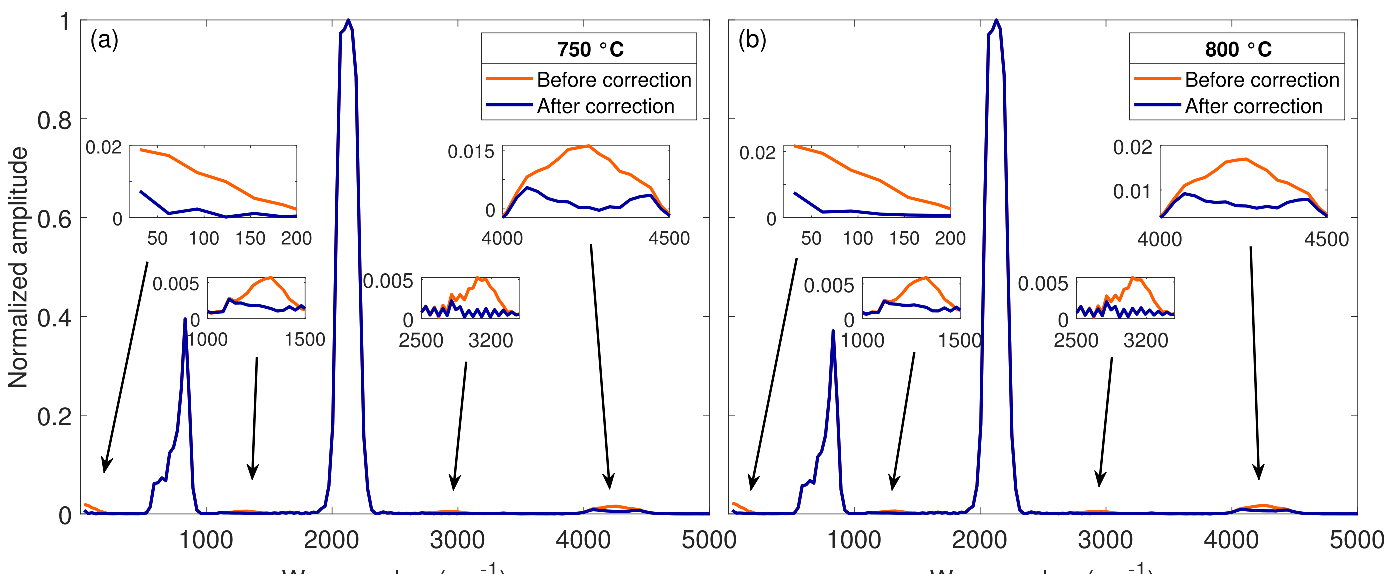

Figure 5. The corrected blackbody spectra at 750 and 800 °C using our method. (a) The results of 750 °C. The amplitudes are corrected fairly in the four out-of-band regions, [0, 400], [1000, 1500], [2500, 3200], and [3800, 4600] cm^{-1}. (b) The results of 800 °C that is similar to panel (a).

and 58.08% in Figure 5 (b), respectively. Table 3 lists all corrected results at different temperatures.

In Table 3, the corrected results, especially at higher temperatures, are more obvious in [0, 400] cm^{-1}. To the artifacts in [1000, 1500] and [2500, 3200] cm^{-1}, although their corrected results are universally worse than these in [0, 400] cm^{-1}, the nonlinearity has been corrected fairly in a way. The worse results are possibly a result of the smaller intensities of their original wave band in [500, 900] cm^{-1} than the spectra in [1900, 2300] cm^{-1}.

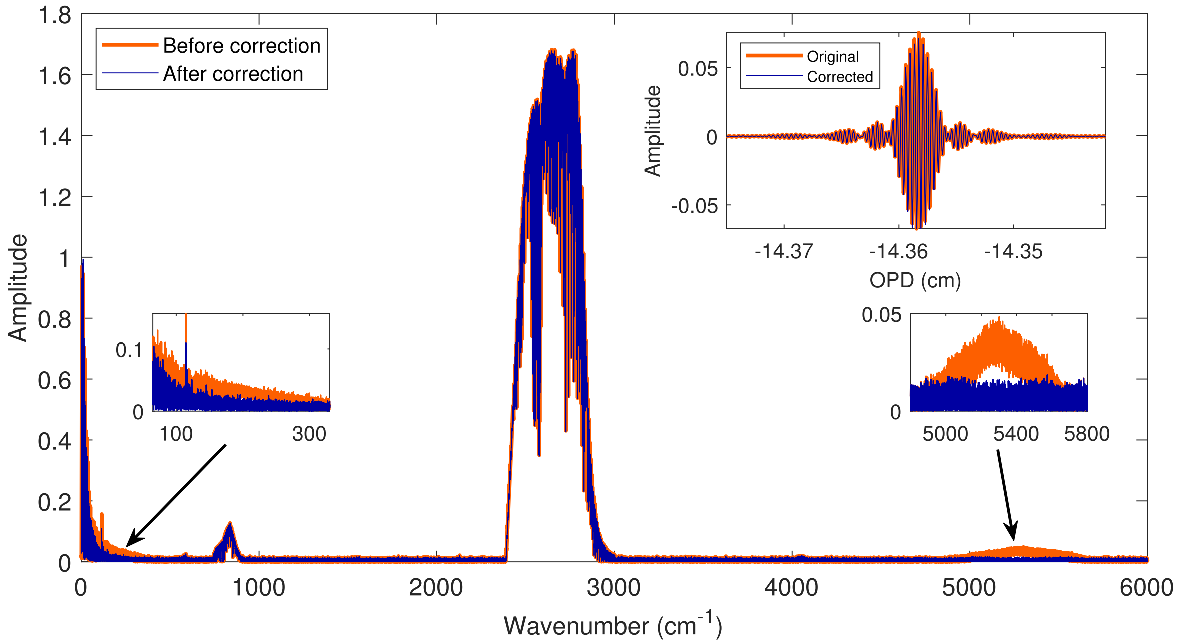

Figure 6. The solar spectrum obtained by the FTS at HSOS and its corresponding interferogram (orange). The filtered wave band is from 2400 to 2900 cm^{-1}, the artifacts are in [0, 500] and [4800, 5800] cm^{-1}. The spectral amplitudes (blue) after correction in these regions are more flatten.

Table 3
The Corrected Results of Spectra at Different Temperatures

Artifacts (cm^{-1})	600 °C	650 °C	700 °C	750 °C	800 °C
[0, 400]	75.30%	71.62%	84.81%	89.09%	87.80%
[1000, 1500]	66.43%	68.19%	70.10%	72.22%	72.50%
[2500, 3200]	72.76%	71.13%	81.39%	83.11%	80.44%
[3800, 4600]	59.46%	65.20%	60.36%	60.84%	58.08%

Finally, we corrected the solar spectrum observed by the FTS at HSOS in [2400, 2900] cm^{-1} wavenumbers whose nonlinear artifacts are located at [0, 500] and [4800, 5800] cm^{-1}. The nonlinearities are enlarged in Figure 6. They are corrected by 65.34% and 81.04% in [0, 500] and [4800, 5800] cm^{-1}, respectively. The corrected interferogram and the corresponding spectra are enlarged and shown in the right of Figure 6.

4. Comparison and Discussion

4.1. Comparison

We compared two nonlinear correction methods, simple iteration (Method 1) and convolution iteration (Method 2) (Lachance 2000; Minzhu et al. 2017), to our method. The two simulated data shown in Figure 1 are again used to achieve Comparison Experiment 1 and 2. The blackbody radiation datum with 750 °C is used to achieve Comparison Experiment 3. All experiments were completed on a Windows 10 64 bit PC with an Intel Core i5 2.60 GHz processor and 32 Gbyte RAM.

Table 4
Performance Evaluation of Different Nonlinear Correction Methods

Dataset	Correction Method	$\lvert a_2 \rvert \times 10^{-1}$	$\lvert \hat{a}_2 \rvert \times 10^{-1}$
Comparison Experiment 1	Method 1	6.000	5.934
	Method 2	6.000	5.934
	Our method	6.000	6.021
Comparison Experiment 2	Method 1	6.000	3.395
	Method 2	6.000	3.213
	Our method	6.000	6.102
Blackbody Comparison	Method 1	⋯	0.024
	Method 2	⋯	0.330
	Our method	⋯	0.112

As the results shown in Table 4, to the two methods (Methods 1 and 2), $\hat{a}_2$ are 5.934×10^{-1} when they reached convergence in a total of 28 and 25 iterations in Comparison Experiment 1. Both have obtained relatively good performances. In Comparison Experiment 2, the two methods have converged after 133 and 58 iterations, respectively. The $\hat{a}_2$ values are 3.395×10^{-1} and 3.213×10^{-1} whose "real" value is 6×10^{-1}. However, our result is 6.102×10^{-1}, demonstrating that our method has better effectiveness. The calculated coefficients of observed blackbody radiation are listed in Table 4.

The comparison results prove that our proposed method has better accuracy, robustness and stability.

4.2. Discussion

Table 3 indicates that the corrected effectiveness is different at various temperatures. The higher temperature, the better corrected effectiveness. Meanwhile, the nonlinear correction for the artifacts in higher out-of-band regions is not obvious compared to others. For example, the corrected results in [3800, 4600] cm^{-1} where the $\overline{P}$ value is only 60.78%, are worse than others in [0, 400], [1000, 1500], and [2500, 3200] cm^{-1}. The reason may be that the dual modulation phenomenon (Lachance 2000; Han et al. 2013), or the intensities in these regions are too small.

In addition, for our method, the calculated quadratic coefficient firmly depends on the optimal interval ([vl, vh] cm^{-1}). Therefore, we need to continuously modify the optimal interval by comparing the spectra before and after correction for a more efficient correction.

5. Conclusion

We first introduced the necessity of the FTS for observing solar activities. However, the interferometer in the FTS exists the nonlinear problem. So we proposed a method using the SA algorithm to correct the FTS nonlinearity. The blackbody spectra with nonlinearity are simulated to evaluate the performance of the proposed method. The experiments indicate that the calculated quadratic coefficient is extremely close to a given value and the difference is only 0.29% in [700, 800] cm^{-1}, demonstrating that our method is more accurate. Meanwhile, our method performs very well in different spectral resolutions and different temperatures, proving that the method holds a good robustness. Finally, we corrected the spectral nonlinearity of the blackbody and solar spectra observed by the FTS at HSOS. The nonlinearity of the blackbody spectra in low- and high-frequency components of the out-of-band is corrected by 89.09% and 60.84%, respectively. The nonlinearity of the solar spectra is corrected by 65.34% and 81.04% in the low- and high-frequency regions of the out-of-band, respectively. All results prove that our proposed method using the SA algorithm can correct the nonlinearity efficiently and can be further used by the FTS of AIMS to improve its accuracy.

Acknowledgments

We thank the temporary and experimental system at HSOS for their FTS data. S.F. is supported by the Joint Funds of the National Natural Science Foundation of China (U1931107). X. Bai is supported by the National Key Research and Development Program of China No. 2021YFA1600500.

ORCID iDs

Song Feng https://orcid.org/0000-0003-4709-7818

References

Bai, X.-Y., Zhang, Z.-Y., Feng, Z.-W., et al. 2021, RAA, 21, 267
Bartoli, F., Allen, R., Esterowitz, L., & Kruer, M. 1974, JAP, 45, 2150
Carangelo, R. M., Hamblen, D. G., & Brouillette, C. R. 1992, Method and system for photoconductive detector signal correction, US Patent No., 5,136,154
Carter, R. O. I., Lindsay, N. E., & Beduhn, D. 1990, ApSpe, 44, 1147
Chase, D. B. 1984, ApSpe, 38, 491
Curbelo, R. 1993, Techniques for correcting non-linearity in a photodetector using predefined calibration information, US Patent No., 5,262,635
Feng, S., Deng, Z., Yuan, D., Xu, Z., & Yang, X. 2020, RAA, 20, 117
Griffiths, P. R. 1983, Science, 222, 297
Han, Y., Revercomb, H., Cromp, M., et al. 2013, JGRD, 118, 12,734
Hoult, R. A., & Ragusa, R. P. 1987, Detector preamplifier for use with a MCT detector, US Patent No., 4,682,022
Jeseck, P., Camy-Peyret, C., Payan, S., & Hawat, T. 1998, ApOpt, 37, 6544
Keens, A., & Simon, A. 1990, Correction of non-linearities in detectors in Fourier transform spectroscopy, US Patent No., 4,927,269
Kirkpatrick, S., Gelatt, C. D., & Vecchi, M. P. 1983, Science, 220, 671
Lachance, R. 2000, Fifth Workshop of Infrared Emission Measurements by FTIR
Learner, R. C. M., Thorne, A. P., & Brault, J. W. 1996, ApOpt, 35, 2947
Metropolis, N., Rosenbluth, A. W., Rosenbluth, M. N., Teller, A. H., & Teller, E. 1953, JChPh, 21, 1087
Minzhu, Y., Yaopu, Z., Lei, Z., & Changpei, H. 2017, Infrared and Laser Engineering, 46, 1023001
Revercomb, H. E., Buijs, H., Howell, H. B., et al. 1988, ApOpt, 27, 3210
Schindler, R. 1986, NASA Tech Briefs, 10, 47
Tobin, D., Revercomb, H., Knuteson, R., et al. 2013, JGRD, 118, 10,589